FULLY AUTOMATIC CAMERA CALIBRATION USING REGULAR PLANAR PATTERNS

V. Douskos [a], I. Kalisperakis [a, b], G. Karras [a], E. Petsa [b]

[a] Laboratory of Photogrammetry, Department of Surveying, National Technical University of Athens (NTUA), GR-15780 Athens, Greece

[b] Department of Surveying, The Technological Educational Institute of Athens (TEI-A), Ag. Spyridonos Str., GR-12210 Athens, Greece - mdouskos@gmail.com, (ilias_k, gkarras)@central.ntua.gr, petsa@teiath.gr

KEY WORDS: Automation, Bundle, Calibration, Distortion, Extraction, Non-Metric

ABSTRACT

Estimation of camera geometry represents an essential task in photogrammetry and computer vision. Various algorithms for recovering camera parameters have been reported and reviewed in literature, relying on different camera models, algorithms and *a priori* object information. Simple 2D chess-board patterns, serving as test-fields for camera calibration, allow developing interesting automated approaches based on feature extraction tools. Several such 'calibration toolboxes' are available on the Internet, requiring varying degrees of human interaction. The present contribution extends our implemented fully automatic algorithm for the exclusive purpose of camera calibration. The approach relies on image sets depicting chess-board patterns, on the sole assumption that these consist of alternating light and dark squares. Among points extracted via a sub-pixel Harris operator, the valid chess-board corner points are automatically identified and sorted in chess-board rows and columns by exploiting differences in brightness on either side of a valid line segment. All sorted nodes on each image are related to object nodes in systems possibly differing in rotation and translation (this is irrelevant for camera calibration). Using initial values for all unknown parameters estimated from the vanishing points of the two main chess-board directions, an iterative bundle adjustment recovers all camera geometry parameters (including image aspect ratio and skewness as well as lens distortions). Only points belonging to intersecting image lines are initially accepted as valid nodes; yet, after a first bundle solution, back-projection allows to identify and introduce into the adjustment all detected nodes. Results for datasets from different cameras available on the Web and comparison with other accessible algorithms indicate that this fully automatic approach performs very well, at least with images typically acquired for calibration purposes (substantial image portions occupied by the chess-board pattern, no excessive irrelevant image detail).

1. INTRODUCTION

Camera calibration (estimation of interior orientation or camera geometry parameters) is a task fundamental to photogrammetry as well as computer vision. Methods for camera calibration (reviewed e.g. by Clarke and Fryer, 1998; Salvi *et al*., 2002; Villa-Uriol *et al*., 2004) may differ in various respects:

- They may involve single or several overlapping images.
- Different camera models may be adopted.
- The observed features may be points but also lines (e.g. Grammatikopoulos *et al*., 2007).
- Both linear and non-linear algorithms may be used.
- Targeted 3D or 2D test-fields are often used, yet camera calibration is also possible with no *a priori* object information.

Indeed, bare image correspondences among >2 frames from the same camera allow self-calibration; however, the use of reliable external control, whenever possible, produces calibration results which stand in close agreement with object space constraints. In addition, for practical close-range photogrammetric tasks it may often be preferable to 'pre-calibrate' a camera through suitable image networks (Remondino and Fraser, 2006).

In this sense, approaches for estimating camera parameters rely usually on test-fields and the correspondences of targets to their images on one or more views. However, 3D test-fields may be replaced by simple 2D patterns, typically of a chess-board type, imaged in several perspective views. If we accept that a camera should ideally be automatically calibrated through rapidly taken image sets (Fiala and Shu, 2005), an essential advantage of such patterns is their suitability for automation, based on feature extraction, thanks to their marked contrast and regularity. Indeed, there exist several freely available tools, employing chess-board patterns recorded in different perspective views, for estimating interior and exterior orientation camera parameters.

These tools have been mainly inspired by 'plane-based calibration' (Sturm and Maybank, 1999; Zhang, 1999), a process relying on the homographies between a plane having known metric structure and its images. The 2D projective transformations produce a linear system in the camera elements; thus, the initialisation step yields a closed-form solution for these parameters, in which lens distortion is generally not included (Sánchez *et al*., 2006). This step is usually followed by a non-linear refinement step, based on the minimization of the total reprojection error.

The *Camera Calibration Toolbox for Matlab*® of J.-Y. Bouguet (implemented also in C++ and included in the Open Source Computer Vision library distributed by Intel) is the best known among the functional tools presented in this context. Initialised through manual pointing of the four chess-board corners on all images and *a priori* information regarding number of nodes per row and column, this algorithm approximates the locations of chess-board nodes on all images and then identifies them with sub-pixel accuracy by an interest point operator (in the presence of strong lens distortion users may be required to approximate its coefficients). Initial approximations for the unknown parameters are supplied by the closed-form plane-based calibration algorithm. Ultimately, an iterative bundle adjustment refines the

solution for camera and pose parameters. Other approaches with higher degree of automation (see the website of Bouguet), some of which represent 'add-ons' to this toolbox, presuppose special target types, non-symmetric chess-board and assumptions about the magnitude of lens distortion, or require that the full calibration pattern appears on the images.

More recently a calibration toolbox has become freely available from the Institute of Robotics & Mechatronics, DLR, Germany (cited *DLR CalDe – DLR CalLab* website). Here the calibration pattern does not have to be fully imaged (thus, in principle, the whole image format may be exploited for the estimation of lens distortion). The procedure runs fully automatically if the chess-board includes three circular targets in its centre, otherwise such points are to be given manually. After a first solution, the user is provided with a tool to identify and remove corners detected erroneously by setting a threshold for image residuals. This step has not been automated (such decisions are regarded as depending to a great extent on the particular cameras).

In the framework described above, our contribution extends the implemented automatic method of Douskos *et al*. (2007) for the exclusive purpose of calibration (image exterior orientations are of no relevance). It relies on image sets of standard chess-board patterns (i.e. light and dark squares of equal size), this being the only *a priori* assumption made. Among extracted image points, only those are kept which may be ordered in two groups of lines referring to the main orthogonal directions of the planar pattern. The subsequent establishment of point correspondences among views is, thanks to the pattern regularity, a trivial task – though possibly involving object systems which differ in in-plane rotation and translations. Yet the fact that homologue image points do not necessarily refer to the same physical node of the pattern affects only exterior orientations. With initial values found from the image vanishing points, a bundle adjustment allows estimating the parameters of camera geometry. After the first solution, back-projection permits to identify possible missing nodes and include them into the final adjustment. The process is described in detail in the next sections. Calibration results from image sets available on the Web are presented and evaluated against those from other calibration toolboxes. It is to note that the algorithm has been tested only with 'reasonable' images taken for calibration purposes (significant perspective differences among views; the pattern occupying substantial parts of the frames; no objects interfering with the imaged pattern).

2. CAMERA CALIBRATION ALGORITHM

The main features of the algorithm, as described in Douskos *et al.* (2007), will be outlined; next, the innovations of the present contribution will be presented.

2.1 Initialisation phase

2.1.1 Corner extraction. After certain experiments with its parameters, the Harris corner operator with sub-pixel accuracy (as made available by Bouguet in his website) is applied to gray-scale images with equalized histograms. Image standard errors of bundle adjustments have corroborated the assertion that the corners are extracted to a precision of ~0.1 pixel. In all tests this step gave quite good results, by extracting practically all pattern nodes and few redundant points. Indications for the satisfactory performance of the sub-pixel Harris operator in cases of chess-board patterns are also found in Ouyang *et al*. (2005).

2.1.2 Point selection and ordering. For each image the median coordinates x_m, y_m of all extracted feature points are calculated; normally, these will indicate a point close to the centre of the pattern. The median, rather than the mean, is preferred due to its lower sensitivity to 'noisy' points outside the pattern area. The feature point closest to M(x_m, y_m) is chosen as a 'base point' B for initialising the point selection and ordering process (Figure 1).

All extracted points around B in a window of size equal to ⅓ of the image size are sorted according to distance from it. If B is a valid node, the principal directions of the pattern must now be identified by avoiding points not corresponding to pattern nodes but also points on chess-board diagonals. The linear segment *s* from B to the nearest extracted point is formed. Identification of the two main pattern directions succeeds by comparing the gray values of pixels on either side of *s* (Figure 1). If segment *s* indeed belongs to one of the two main chess-board directions, a large difference in gray values between either sides of *s* is expected. The representative gray value on either side is calculated from a sample along a line parallel to *s*, with length equal to ⅓ of the length of *s* and with its midpoint distanced half the length of *s* away from the midpoint of *s*. In case the difference between the mean gray values of these samples on either side of *s* is found to exceed the overall standard deviation of image gray values by more than a factor of 3, this segment *s* is accepted as belonging to one of the principal chess-board directions.

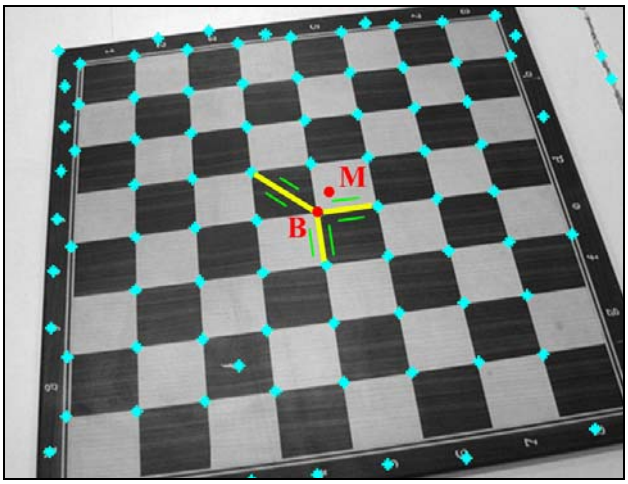

Figure 1. Extracted points (cyan); 'median' (M) and 'base' (B) points; possible directions (yellow); auxiliary lines (green) used for checking the validity of directions.

This is repeated for the next 7 closest points around B. If the other principal direction (perpendicular to the first on the chess-board) is also found, the two segment lengths and directions are stored as initial reference values, and the algorithm continues to identify the rows and columns of the pattern. If it is not possible to establish both directions, this 'base point' B apparently does not represent a chess-board node (or only few points are around it). The process is resumed by using as new 'base point' B that next closest to M. This procedure is continued until both main directions have been established.

A similar search evolves as regards the adjacent points on these two lines. Using the stored values for segment length and angle of the respective main direction, the position of the next point on the line is anticipated. The algorithm searches within a small region (fixed by thresholds in segment length and angle) around

the estimated point position to locate extracted feature points. If a point is found, it is considered as belonging to the same line (optionally the gray-value criterion can also be used here, but in all performed tests this has not been necessary). This point now represents a 'base point' for the next search. Values for segment length and slope are updated accordingly; next segments define new search lengths and slopes. It is noted that here – as opposed to approaches where the estimation of point locations relies on the manual introduction of the four corner points of the chess-board – the effect of lens distortion on the directions defined by neighbouring nodes on a line is regarded as negligibly small.

It is not necessary to locate every individual node of the pattern. In case of a missing node, the position of the next one is estimated, and an acceptable extracted point is again searched for. If three successive 'missing points' are encountered, it is assumed that all points of a line have been found and the search is halted. This is repeated for locating all points of the orthogonal pattern line. Lines with less than four points are regarded as unreliable, and a 'gap' is considered in their place.

Next, from the central point of the first line (via the orthogonal direction and the corresponding segment length) the location of a point of the next parallel line is estimated. If a point is found, the same process is continued; else, starting from points next to this central point, corresponding points on the parallel line are searched for. If it is not possible to locate points on this line, a 'gap' is set in its place, and the algorithm continues to look for a point of the next parallel line. When having encountered three successive 'gaps', the algorithm accepts that no further lines are detectable in this direction, and continues with a similar search for converging image lines (i.e. parallel pattern lines), steered as before by local segment length and direction.

After the detection process for pattern lines is terminated, these are ordered. The pattern line through the original 'base point' B which forms the smaller angle with the image x-axis establishes the set of 'rows'; the other line fixes the 'columns'. Rows and columns are then sorted according to the coordinate of their intersection with the respective image axis (x for columns and y for rows). As a basic precaution, in Douskos *et al*. (2007) only points which belong to both a row and a column are accepted as valid chess-board nodes. This allows excluding outliers, namely points (particularly outside the pattern) which might happen to be roughly collinear with a chess-board line, while at the same time their distance from a point of the line falls within the local tolerance of segment length. Such a measure to discard possible blunders is indispensable to ensure convergence in bundle adjustment. As outlined below, however, an additional last step is introduced here in order to exploit all available extracted chess-board corners in a subsequent final solution for calibration.

In Figs. 2 and 3 some examples are presented – from two of the image sets used for the practical evaluation and documented in Section 3 – which illustrate the three basic steps outlined so far (namely, point extraction, line formation and selection of chess-board nodes). One may note there that, thanks to an appropriate choice of the parameters of the point operator, only few points outside the pattern are extracted. Nonetheless, it is seen that in some cases (top and bottom images in Figure 2) points beyond the limits of the pattern are initially assumed as belonging to a line; such points are subsequently excluded, since they are not found to belong to both a column and a row of the grid (right column in Figure 2 and Figure 3). Yet, it is obvious in these Figures that this necessary measure tends to 'decimate' the valid nodes, mainly near the image edges, and thus actually 'narrows' the bundle of rays. Such valid nodes are later 'regained' by the algorithm, as explained in Section 2.2.2. A final remark is also to be made as regards the chess-board of Figure 3. This particular pattern carries three near-circular targets at its centre (intended to fix the object reference system). In some cases the algorithm is 'disturbed' by points extracted on these targets; as a consequence, certain rows and columns display significant 'gaps' (this is clearly illustrated in the second image of Figure 3). These points are, too, regained later (cf. Figure 5).

2.1.3 Point correspondences.

Final outcome of preceding steps is a set of points coded according to the respective chess-board rows and columns with which they have been associated (right column in Figs. 2 and 3). The lower row appearing on an image is defined as 'Row 1' and is arbitrarily considered as coincident with the object X-axis; the column to the far left is defined as 'Column 1' and is associated with the object Y-axis. Thus, the node which belongs to these two lines is now point (1,1) of this particular image and is associated with the origin (point 1,1) of the chess-board XY system. If the intersection of the first row and column (point 1,1) does not actually appear on an image, or has not been detected, the adjacent node detected on this image is numbered accordingly, e.g. (2,1) or (1,2) etc. The process is repeated for all images. Hence – thanks to the symmetric nature of the pattern – it may be assumed that point correspondences among frames, as well as correspondences with the chess-board nodes, have been fully established. In our context, this provides an answer to the problem of correspondences, which is regarded as the most difficult part in automatic camera calibration and is often solved manually (Fiala and Shu, 2005).

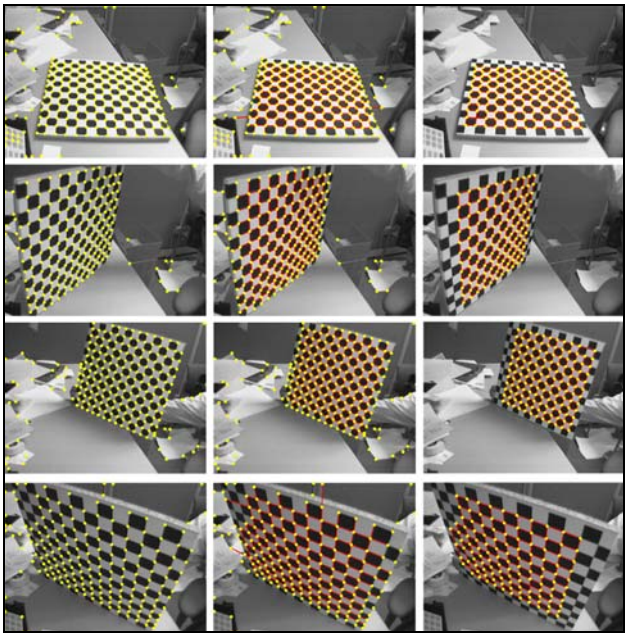

Figure 2. Four examples from the image set of Bouguet. *Left*: Initially extracted points. *Centre*: Points ordered along the two principal directions. *Right*: Only points belonging both to a row and a column are kept.

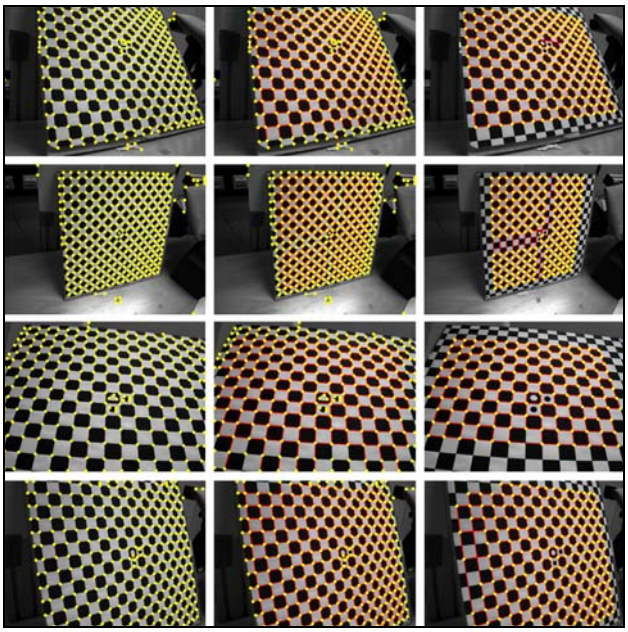

Figure 3. Four examples from the image set of DLR (camera I). *Left*: Initially extracted points. *Centre*: Points ordered along the two principal directions. *Right*: Only points belonging both to a row and a column are kept.

Evidently, exterior orientations (image pose) are irrelevant here. The images refer to their own object systems, which may differ by in-plane shifts and rotations. Consequently, the point correspondences among views established above *will not necessarily refer to identical physical points* of the pattern. But this can be ignored, thanks to the symmetry of the chess-board. In fact, in a camera calibration process with 2D control it is the perspective distortions of images which really matter, i.e. their relation to the planar object and not to a system fully fixed in object space.

It is to note that this approach – in which images acquired from different sides of the pattern are possibly treated as taken from the same side – has its effect on ray intersection angles in self-calibration. If no ground control is used, this will be reflected in the precision of interior orientation parameters (Douskos *et al*., 2007, have presented results without ground control). But since our approach presupposes pattern squares of equal size, object coordinates (arbitrarily scaled) may be introduced in bundle adjustment. If these are treated as error-free (or highly weighted), the independent selection of a 2D system for each image is not expected to significantly affect precision of camera calibration.

On the other hand, it is well-known that orthogonal image roll angles (κ) weaken correlations between the elements of interior and exterior orientation. Clearly, our approach is inherently incapable of recognizing such rotations – a price paid for employing plain chess-board patterns without special targeting for the orientation of the object system. Interchange of X and Y object axes in some images might provide a possible answer. In a test reported in Douskos *et al*. (2007) this has significantly loosened larger correlations (of y_o with rotations ω and κ) at the expense of an increase in the smaller correlations (of y_o with ϕ, and of x_o with ω and κ). This is a point for further investigation.

2.1.4 Initial values. Instead of a direct solution via plane-based calibration, estimation of approximate values for the unknowns is based here on the vanishing points (VP) of the two principal chess-board directions. These are found by line-fitting to points already classified in pencils of converging image lines. For each direction, an initial estimate of VP location is obtained from the two lines with >3 points forming the largest angle. In case the distance of some VP from the image centre exceeds the image size by a factor of 40 (which corresponds to a rotation angle of ~1.5° for moderately wide-angle lenses), this VP is considered at infinity. If both VPs are finite, their locations are refined in a single adjustment, in which coefficients of radial lens distortion are also included as unknowns. Using diagonals with >3 points, the VP of the diagonal direction of the pattern falling between the two main VPs is also included as an unknown to enforce the vanishing line constraint. If only one VP is finite, it is estimated from all participating lines along with the coefficients of radial distortion. It is noted that this approach supplies simultaneously good estimates for the radial distortion coefficients.

Assuming that the principal point is at the image centre, camera constant c and image rotation matrix may be estimated through the two principal VPs of each image (Karras *et al*., 1993). The estimates of camera constant c and of the distortion coefficients with smallest standard error (σ_c is estimated by error propagation) are used as initial values in bundle adjustment. If one of the two VPs is close to infinity, the corresponding out-of-plane rotation (ω or ϕ) is set to zero, the other is found by using the mentioned 'best' value for c; estimation of roll angle κ is trivial.

Coming now to the approximation of parameters of image pose, the largest dimension in X seen on all images is chosen, scaled arbitrarily, to estimate camera altitudes (Karras *et al*., 1993). In the XY system of each image, the location of projection centre is then estimated through the image coordinates of the origin (point 1,1). In case this latter point has not been detected on an image, it is found as the intersection of row 1 and column 1.

2.2 Bundle adjustment

Having determined image-to-pattern point correspondences and initial parameter values, an iterative bundle adjustment is then carried out for estimating camera geometry.

2.2.1 Mathematical model. The model employed here adopts a typical camera matrix (Hartley and Zisserman, 2000), i.e. next to camera constant c and principal point location (x_o, y_o) it also incorporates image aspect ratio – equivalently camera constants c_x, c_y – and image skewness s. Coefficients k_1 and k_2 for radial symmetric lens distortion are, too, present. Coefficients p_1, p_2 of decentering distortion also take part, although in current digital cameras this error appears as mostly negligible when compared to sensor quantisation, and thus represents a possible source of instability (Zhang, 1999) – a phenomenon also met in our tests (values hardly exceeding 1 pixel in the useful image area). The distortion model of Brown (1966) is used here, with image radii referring to corrected image coordinates. Finally, it is noted that the algorithm may also function in a pure self-calibration mode, i.e. without control (Douskos *et al*., 2007 have presented such tests). For reasons already referred to, results presented below rely on control points with coordinates assumed as error-free.

2.2.2 Refinement through back-projection. As mentioned, the first solution is performed using only points identified on both a row and a column of the pattern (right column in Figs. 2 and 3), as a 'double-check' on the validity of identified nodes. Besides few extracted nodes in the central part of the pattern which have been excluded for some reason (as in the case of the additional targets of Figure 3), the discarded nodes are mainly situated on the outer rows and columns, thus producing 'narrower' bundles.

A remedy is to recover such valid nodes by back-projection of the XY node coordinates onto the images.

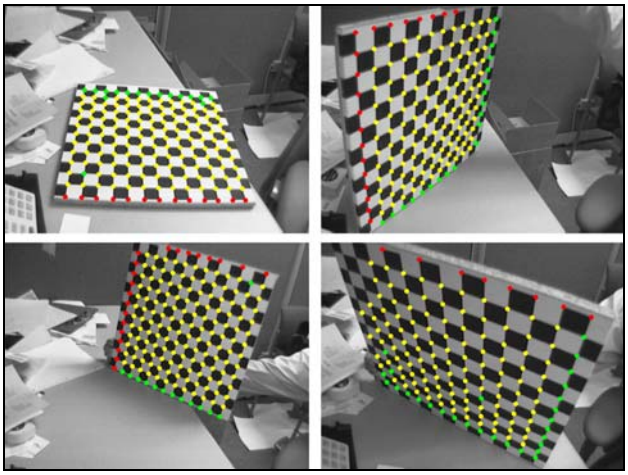

Figure 4. Additional valid nodes (in green and red) identified on the four images of Figure 2 and introduced in the final adjustment.

Thus, using the information gained from the first bundle adjustment, pattern nodes are back-projected as follows. First, among the total of the already established chess-board nodes (i.e. nodes identified on at least one image) all missing nodes are projected on each image. A search for extracted points within a window around the projected node thus allows detecting missing nodes. Here the window size is ~2×2 pixels ($\pm 10 \times \sigma_o$), but an adaptive window might also be used based on local image scale. Besides, it is checked whether these points also belong to a column or a row. Such recovered nodes are seen in Figs. 4 and 5 marked in green. It is observed that in some instances, as in the case of the top right image in Figure 5, significant portions of columns and of rows may be 'regained' in this manner.

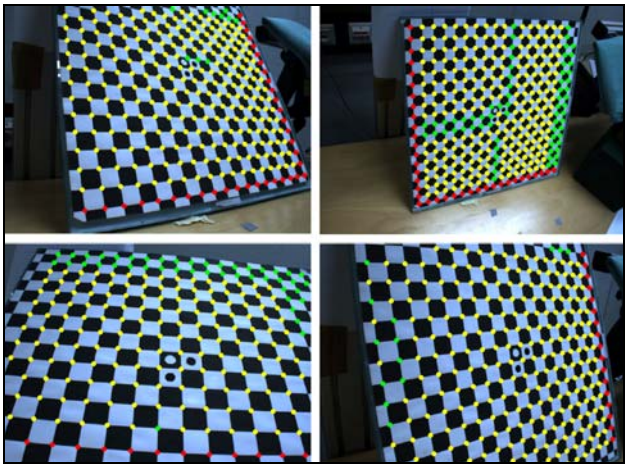

Figure 5. Additional valid nodes (in green and red) identified on the four images of Figure 3 and introduced in the final adjustment.

Second, three additional rows and columns on either side of the identified chess-board edges are projected on all images. This is intended to find acceptable outer rows or columns of the pattern which may have not been found up to now, in order to 'widen' the bundles of rays. The same search scheme is adopted here. It is noted that isolated nodes are not kept, namely only new rows or columns with a certain number of points (>6) are accepted; yet these points do not have to be successive, i.e. 'gaps' may be tolerated. It is seen in Figs. 4 and 5, where such points appear in red, that it has been indeed possible to establish such new lines.

Using all identified points, a final bundle adjustment for camera calibration is carried out.

3. TESTS AND EVALUATION

The original implementation of the approach has been applied successfully to various cameras by Douskos *et al*. (2007), who also showed that under circumstances the method is applicable to moderately asymmetric patterns, like those of Zhang (1999). Further, results were also shown from three image sets available in Internet, for which there exist results from other toolboxes. In the present evaluation the same three image sets were used with the current implementation of the algorithm (inclusion of image skewness and addition of possibly all nodes via reprojection).

• ***Image set 1.*** The algorithm has been applied to the 25 images (640×480) available in the web site of J.-Y. Bouguet (4 of these are seen in Figure 2). Results are shown in Table 1.

	A	*B*
σ_o (pix)	0.12	0.12
c_x (pix)	657.31 ± 0.11	657.30 ± 0.10
c_y (pix)	657.76 ± 0.11	657.74 ± 0.10
x_o (pix)	−16.81 ± 0.21	−17.28 ± 0.20
y_o (pix)	−3.46 ± 0.20	−2.33 ± 0.19
$s(\times 10^{-03})$	−0.33 ± 0.07	−0.42 ± 0.06
$k_1(\times 10^{-07})$	−5.89 ± 0.02	−5.87 ± 0.02
$k_2(\times 10^{-13})$	6.69 ± 0.19	6.34 ± 0.17
$p_1(\times 10^{-06})$	0.02 ± 0.07	0.08 ± 0.07
$p_2(\times 10^{-06})$	0.45 ± 0.07	0.43 ± 0.06

Table 1. Calibration results for image set 1
A: our algorithm; B: Bouguet's toolbox

Included in Table 1 (B) are also the corresponding results given for the same images by Bouguet using his *Camera Calibration Toolbox for Matlab®*. Since in this latter solution the two outer rows of the pattern had not participated, we have also excluded from our adjustment these rows (found via back-projection) to obtain results which will be directly comparable. Furthermore, in the results from the Bouguet toolbox as presented in Table 1, the distortion coefficients have been reduced by corresponding powers of c to become compatible with our model; the principal point location (x_o, y_o) has been referred to the image centre; the signs of skewness s and coefficient p_2 are reversed to agree with the right-handed image system used in photogrammetry; finally, σ_o stands for the 'reprojection error'.

It is seen that results for all parameters from the two algorithms are practically identical. Differences in s or p_1 are insignificant, and so is the difference of 1 pixel in the principal point location, particularly since the variability of principal point estimations is generally regarded as high compared to other camera elements (Ruiz *et al*., 2002). The radial distortion curves are coincident.

• ***Image sets 2 and 3***.
The algorithm has also been evaluated on a group of 10 stereo pairs (780×580) from the *DLR CalDe–DLR CalLab* website. The pairs stem from two different cameras and are treated here as two separate sets from independent cameras I and II (4 images from camera I are in Figure 3). It is noted that the pattern is recorded only in part on certain images. Results have

been concentrated in Table 2, where also corresponding results from the *DLR CalDe–DLR CalLab* software (B), run in single-image mode, are included. Again, parameters mentioned above have been transformed to comply with our distortion model and also for reversing the left-handed system of the digital images usually used in 'non-photogrammetric' calibration toolboxes. It is also pointed out that this particular software does not supply standard errors of parameters.

	Camera I		Camera II	
	A	*B*	*A*	*B*
σ_o (pix)	0.11	0.14	0.11	0.14
c_x (pix)	727.75 ± 0.08	727.28	732.05 ± 0.08	731.57
c_y (pix)	726.98 ± 0.07	726.45	730.98 ± 0.08	730.42
x_o (pix)	–14.52 ± 0.10	–14.81	–19.18 ± 0.10	–19.23
y_o (pix)	–0.19 ± 0.09	0.92	–5.07 ± 0.09	–3.84
$s(\times 10^{-03})$	2.38 ± 0.03	2.39	2.23 ± 0.03	2.23
$k_1(\times 10^{-07})$	–3.85 ± 0.01	–3.87	–3.94 ± 0.01	–3.99
$k_2(\times 10^{-13})$	3.61 ± 0.03	3.68	4.13 ± 0.03	4.36
$p_1(\times 10^{-06})$	0.64 ± 0.04	0.75	0.21 ± 0.04	0.34
$p_2(\times 10^{-06})$	2.10 ± 0.04	2.33	0.42 ± 0.04	0.78

Table 2. Calibration results for image sets 2 and 3
A: our algorithm; B: DLR CalDe–DLR CalLab toolbox

In a strict sense, results from the two algorithms are not directly comparable, since when running the *DLR CalDe–DLR CalLab* software some dozens of erroneous points near the image edges had to be discarded to obtain reasonable reprojection error. Yet, here again the calibration results stand in quite good agreement.

4. CONCLUDING REMARKS

Extending the algorithm of Douskos *et al*. (2007), an approach has been presented for the automatic multi-image calibration of cameras from images of plain chess-board patterns – under one single assumption, namely that these consist of adjacent equally sized squares. After the first solution, back-projection of object nodes allowed a considerable increase (which for image sets 2 and 3 exceeded 20%) of the number of points participating in the final adjustment. Camera calibration results, using imagery from different Web sources, are considered as being essentially identical to calibration data available from other camera calibration methods, relying on planar test-fields. Characteristic for the approach is the fact that exterior orientation is of no relevance, due to the symmetry of the pattern. Being fully automatic, the presented algorithm presupposes that 'reasonable' – in quality, pattern coverage as well as in number – image sets are at hand, having significant differences in perspective to constitute strong configurations.

This question of 2D projectivity is indeed central in all related approaches, including of course those which rely explicitly on homograhies (plane-based calibration). Thus, it is projectivities and not the particular exterior orientations which matter. In our approach where image pose *per se* is not relevant, for instance, one and the same image may well have been acquired with four different symmetric exterior orientations; clearly, this does not imply that a single image of a 2D pattern (a given projectivity) may 'pretend' to be four different images, and hence sufficient for 'multi-image' camera calibration. In this sense, studying the combinations of the projectivities optimal for estimating camera geometry is a very interesting question. With camera calibration by means of 2D patterns being an attractive simple approach of high potential, this aspect has to be further investigated.

REFERENCES

Bouguet J.-Y.: *Camera Calibration Toolbox for Matlab*, http://www.vision.caltech.edu/bouguetj/calib_doc/

Brown D.C., 1966. Decentering distortion of lenses. *Phot. Eng.*, 32(3), pp. 444-462.

Clarke T.A., Fryer J.G., 1998. The development of camera calibration methods and models. *Phot. Rec.*, 16(91), pp. 51-66.

DLR CalLab – CalDe Software: http://www.dlr.de/rm/desktopdefault.aspx/tabid-1524/

Douskos V., Kalisperakis I., Karras G., 2007. Automatic calibration of digital cameras using planar chess-board patterns. 8th Conf. Opt. *3-D Meas. Techn.*, Wichmann, vol. I, pp. 132-140.

Fiala, M., Shu, C., 2005. Fully Automatic Camera Calibration Using Self-Identifying Calibration Targets. *Techn. Rep.* 48306/ ERB-1130, NRC Canada, pp. 26.

Grammatikopoulos L., Karras G., Petsa E., 2007. An automatic approach for camera calibration from vanishing points. *ISPRS J.* Phot. Rem. Sens, 62, pp. 64-76.

Hartley, R., Zisserman, A., 2000. *Multiple View Geometry in Computer Vision*. Cambridge University Press.

Karras G., Patias P., Petsa E., 1993. Experiences with rectification of non-metric digital images when ground control is not available. Proc. XV Int. CIPA Symp., Bucharest (unpaginated).

Ouyang C., Wang G., Zhang Q., Kang W., Ding H., 2005. Evaluating Harris method in camera calibration. 27th *IEEE Eng. in Med. & Biol. An. Conf.*, Shanghai, Sept. 1-4, pp. 6383-6386.

Remondino F., Fraser C., 2006. Digital camera calibration methods: considerations and comparisons. Int. Arch. Phot. Rem. *Sens. & Spatial Sciences*, 36(5), pp. 266-272.

Ruiz A., López-de-Teruel P.E., García-Mateos G., 2002. A note on principal point estimability. Proc. 16th *ICPR*, Aug. 11-15, Quebec, vol. 2, pp. 304- 307.

Salvi J., Armangué X., Batlle J., 2002. A comparative review of camera calibrating methods with accuracy evaluation. *Pattern Recognition,* 35, pp. 1617-1635.

Sánchez J.A., Destefanis E.A., Canali L.R., 2006. Plane-based camera calibration without direct optimization algorithms. IV Jornadas Argentinas de Robótica, Córdoba, 16 -17 November.

Sturm P.F., Maybank S.J., 1999. On plane-based camera calibration: a general algorithm, singularities, applications. *IEEE Conf. CVPR'99*, Fort Collins, USA, pp. 432-37.

Villa-Uriol M.-C., Chaudhary G., Kuester F., Hutchinson T. C., Bagherzadeh N., 2004. Extracting 3D from 2D: selection basis for camera calibration. *IASTED Comp. Graph. & Imag.*, Kauai, USA, pp. 315-321.

Zhang Z., 1999. Flexible camera calibration by viewing a plane from unknown orientations. *IEEE. Conf. ICCV '99*, Corfu, pp. 666-673.